

# Pion condensation versus 2SC, speed of sound, and charge neutrality effects in the quark-meson diquark model

Jens O. Andersen<sup>1,\*</sup> and Mathias P. Nødtvedt<sup>1,†</sup>

<sup>1</sup>*Department of Physics, Faculty of Natural Sciences, NTNU,  
Norwegian University of Science and Technology, Høgskoleringen 5, N-7491 Trondheim, Norway*  
(Dated: February 17, 2025)

We employ the two-flavor quark-meson diquark model as a low-energy model for QCD at non-zero quark and isospin chemical potentials  $\mu$  and  $\mu_I$ , and at zero temperature. We map out the phase diagram in the  $\mu$ - $\mu_I$  plane, which has four phases: a vacuum phase, a phase with condensed charged pions/Cooper pairs of  $u$  and  $\bar{d}$  quarks, a normal quark matter phase, and a color superconducting phase (2SC phase). The global symmetry breaking  $SU(3)_c \rightarrow SU(2)_c$  in the 2SC phase gives rise to a number of Nambu-Goldstone bosons. We classify them and briefly discuss their properties. We calculate the speed of sound  $c_s$  in the two special cases, finite  $\mu_I$  and  $\mu = 0$ , and finite  $\mu$  and  $\mu_I = 0$ . In both cases, the speed of sound exhibits a maximum and approaches the conformal limit from above as the density increases. For non-zero isospin  $\mu_I$ , this behavior is in agreement with the speed of sound obtained from lattice simulations. In the 2SC phase, the behavior is qualitatively the same if we impose local charge neutrality. Finally, we discuss the possibility of having a mixed phase of negatively charged normal quark matter and positively charged 2SC matter with global color charge neutrality imposed on the latter.

## I. INTRODUCTION

QCD in extreme conditions has been of interest for decades due to its relevance to the early universe, heavy-ion collisions, and compact stars [1–3]. The QCD phase diagram, which conventionally is drawn in the  $\mu$ - $T$  plane, turns out to be very rich, with a number of phases. It becomes even more complicated if we allow an independent chemical potential for each quark flavor  $f$  instead of a common baryon chemical potential. For two quark flavors, we can then use  $\mu_u$  and  $\mu_d$  or equivalently use the isospin chemical potential  $\mu_I = \mu_u - \mu_d$  and the baryon chemical potential  $\mu_B = 3\mu$ . For three flavors, we add a  $\mu_S$ -axis, where  $S$  is strangeness, and  $\mu_S = \frac{1}{2}(\mu_u + \mu_d - 2\mu_s)$ . Consider the phase diagram in the  $\mu_B$ - $\mu_I$  plane. Moving along the  $\mu_I$ -axis, QCD is in the vacuum phase until the isospin chemical potential reaches the critical value  $\mu_I^c = m_\pi$  where one expects the onset of charge pion condensation [4]. For sufficiently small values of  $\mu_I$ , the pion-condensed phase can be described in a model-independent way using chiral perturbation theory [5, 6]. For very large values of  $\mu_I$ , quarks and gluons are the relevant degrees of freedom, and if the density is sufficiently high, one can use perturbative QCD (pQCD). In pQCD, one-gluon exchange gives rise to an attractive quark-quark interaction channel. According to BCS theory for superconductivity, any attractive interaction renders the Fermi sphere unstable, and Cooper pairs are formed. Since  $\mu_u = -\mu_d$ , these pairs consist of  $u$  quarks and  $\bar{d}$  antiquarks or vice versa depending on the sign of  $\mu_I$ . Thus, QCD at very large isospin chemical potential is a color superconductor. The diquark condensate or the gap has the same quantum numbers as those

of the pion condensate that exists for low values of  $\mu_I$ , so one expects a BEC-BCS crossover transition as one increases  $\mu_I$  [4]. A nice feature of QCD at non-zero  $\mu_I$  but  $\mu_B = 0$  is the absence of the sign problem and the possibility to perform lattice simulations. It is then possible to compare lattice QCD [7–9] with model-independent predictions for small  $\mu_I$  using chiral perturbation theory [4, 10] and perturbative QCD for large  $\mu_I$ .

The situation is similar at large baryon chemical potentials, where perturbative QCD can be applied. Again, there is an attractive channel that involves one-gluon exchange. For sufficiently large values of  $\mu_B$ , all three quark flavors can be taken massless, and they participate in the pairing on an equal footing as do the quarks of different colors. The resulting ground state is referred to as the color-flavor-locked (CFL) phase of QCD, whose existence at asymptotically large baryon chemical potential is one of the few rigorous results in cold and dense QCD. Moving towards smaller values of  $\mu_B$ , one can no longer ignore the mass of the  $s$ -quark. The finite value of  $m_s$  places stress on pairs that contain an  $s$ -quark. Eventually, it is energetically advantageous to break up such pairs, and one is left with a pairing pattern that involves the  $u$  and  $d$  quarks and two of the three colors. This phase is referred to as the 2SC phase.<sup>1</sup> Note, however, that the existence of the 2SC phase depends on the details of the models employed. For example, in the NJL model, there is a 2SC phase between the phase of normal quark matter and the CFL phase, if the couplings are small. For larger values of the couplings, the transition from the CFL phase directly to normal quark matter [12–14].

\* jens.andersen@ntnu.no

† mathias.p.nodtvedt@ntnu.no

<sup>1</sup> Before the breakup of Cooper pairs, the stress on them may be relieved by kaon condensation. The system is still in the CFL phase, but the condensation corresponds to a rotation of the order parameter [11].

The interest in QCD at finite quark chemical potentials and low temperature is mainly due to its applications to compact stars. Knowing the equation of state allows us to calculate macroscopic quantities such as masses and radii of individual neutron stars as well as tidal deformabilities in binary systems. The recent observations of compact stars of more than two solar masses put constraints on the equation of state and one of the main questions is whether the most massive stars have a quark core surrounded by ordinary nuclear matter. The quest for a phase transition in dense QCD has been hampered by the inapplicability of lattice QCD at finite  $\mu_B$  due to the sign problem. The sign problem forces one to use other methods. At very large values of the baryon chemical potential, perturbative QCD (pQCD) is applicable due to asymptotic freedom. In recent years, perturbative calculations have been pushed to order  $\alpha_s^3 \log \alpha_s$ , where  $\alpha_s$  is the strong coupling [15, 16]. In Ref. [17], renormalization group methods have been used to improve the convergence of perturbative series. For lower values of  $\mu$ , where pQCD cannot be applied, one uses low-energy effective models that in some aspects resemble QCD. The

Nambu-Jona-Lasinio model is an example of a low-energy effective model that incorporates chiral symmetry breaking in the vacuum, but has no dynamical gauge fields. The local  $SU(3)_c$  gauge symmetry is then replaced by the corresponding global symmetry.

The present work is a continuation of Ref. [18]. In that paper, we formulated the two-flavor quark-meson diquark (QMD) model as a renormalizable low-energy effective model for two-flavor QCD, with meson, quark, and diquark degrees of freedom. In this paper, we continue our study of the model and its properties, focusing on the phase diagram in the  $\mu_I$ - $\mu_B$  plane, the speed of sound, and the effects of imposing neutrality for electric and color charge.

## II. TWO-FLAVOR QMD MODEL

### A. Lagrangian

The Minkowski Lagrangian for the two-flavor quark-meson diquark model is

$$\begin{aligned} \mathcal{L} = & \frac{1}{2}(\partial_\mu \sigma)(\partial^\mu \sigma) + \frac{1}{2}(\partial_\mu \pi_0)(\partial^\mu \pi_0) + (\partial_\mu + i\mu_I \delta_{\mu 0}) \pi^+ (\partial^\mu - i\mu_I \delta^{\mu 0}) \pi^- - \frac{1}{2}m^2(\sigma^2 + \vec{\pi}^2) - \frac{\lambda}{24}(\sigma^2 + \vec{\pi}^2)^2 \\ & + h\sigma + (\partial_\mu + 2i\mu_a \delta_{\mu 0}) \Delta_a^\dagger (\partial^\mu - 2i\mu_a \delta^{\mu 0}) \Delta_a - m_\Delta^2 \Delta_a^\dagger \Delta_a - \frac{\lambda_3}{12}(\sigma^2 + \vec{\pi}^2) \Delta_a^\dagger \Delta_a - \frac{\lambda_\Delta}{6} (\Delta_a^\dagger \Delta_a)^2 \\ & + \bar{\psi}(i\not{\partial} + \gamma^0 \hat{\mu})\psi - g\bar{\psi}[\sigma + i\gamma^5 \vec{\pi} \cdot \vec{\tau}]\psi + \frac{1}{2}g_\Delta \bar{\psi}_b^C \Delta_a \gamma^5 \tau_2 \epsilon_{abc} \psi_c + \frac{1}{2}g_\Delta \bar{\psi}_b \Delta_a^\dagger \gamma^5 \tau_2 \epsilon_{abc} \psi_c^C, \end{aligned} \quad (1)$$

where  $\psi$  is a flavor doublet and a color triplet in the fundamental representation

$$\psi = \begin{pmatrix} \psi_{ur} \\ \psi_{dr} \\ \psi_{ug} \\ \psi_{dg} \\ \psi_{ub} \\ \psi_{db} \end{pmatrix}. \quad (2)$$

Furthermore,  $\psi_c$  is the flavor doublet with color  $c$

$$\psi_c = \begin{pmatrix} \psi_{uc} \\ \psi_{dc} \end{pmatrix}. \quad (3)$$

The field  $\Delta_a$  is a composite diquark field,  $\Delta_a \sim \bar{\psi}_b \tau_2 \epsilon_{abc} \gamma^5 \psi_c^C$ , where  $\psi^C = C\bar{\psi}^T$  and  $C = i\gamma^2 \gamma^0$  is the charge conjugation operator, which can be written as

$$\Delta = \begin{pmatrix} \Delta_1 \\ \Delta_2 \\ \Delta_3 \end{pmatrix}. \quad (4)$$

The diquark field  $\Delta$  transforms as a singlet under  $SU(2)_L \times SU(2)_R$  and as an antitriplet under  $SU(3)_c$ .

Furthermore,  $\hat{\mu}$  is the quark chemical potential matrix,  $\mu_I$  is the isospin chemical potential for electrically charged pions, and  $\mu_a$  is the chemical potential for diquark  $a$ . The chemical potentials  $\hat{\mu}$ ,  $\mu_a$ , and  $\mu_I$  are not independent, but can be expressed in terms of  $\mu_B$ ,  $\mu_e$ , and  $\mu_8$  which are the chemical potentials for baryon number, electric charge, and color charge  $Q_8$  (see subsection II B). The symmetries of the Lagrangian in Eq. (1) were discussed in some detail in Ref. [18], here we simply state them. In the chiral limit, the global symmetries are  $SU(2)_L \times SU(2)_R \times U(1)_B \times SU(3)_c$ , while at the physical point, the global symmetry is  $SU(2)_V \times SU(3)_c$ . The diquark condensate  $\Delta_0 = \langle \Delta_3 \rangle$  in the 2SC phase breaks the  $SU(3)_c$  to  $SU(2)_c$ . The  $U(1)_B$  symmetry in the vacuum, which is generated by  $B = \frac{1}{3} \text{diag}(1, 1, 1)$  is modified in the medium,  $\tilde{B} = B - \frac{2}{\sqrt{3}} T_8 = \text{diag}_c(0, 0, 1)$ , where  $T_a$  are the generators of  $SU(3)$ . In the 2SC phase, only the blue quasiparticles carry a non-zero  $\tilde{B}$  charge [19]. Similarly, there is an unbroken modified  $U(1)$  symmetry generated by  $Q' = Q - \frac{1}{\sqrt{3}} T_8$ , where  $Q = \text{diag}(\frac{2}{3}, -\frac{1}{3})$  is the generator of the electromagnetic  $U(1)$  symmetry. In the QMD model, this symmetry is global, whereas in QCD it is local. The gauge boson associated with this symmetry is then the in-medium photon. In the condensed phase of

the pion, the condensate  $\bar{\rho}_0$  breaks the symmetry  $U(1)_{I_3}$  associated with the third component of the isospin, that is, the subgroup of  $SU(2)_V$ . The  $U(1)$  electromagnetic symmetry is also broken since  $I_3 = Q + \frac{1}{6}\mathbb{1}$ .

The Lagrangian has a number of masses and couplings. They can be grouped whether they belong to the quark-meson sector or the diquark-meson sector. The former include  $m^2$ ,  $\lambda$ ,  $g$ , and  $h$ , while the latter includes  $m_\Delta^2$ ,  $\lambda_3$ ,  $\lambda_\Delta$ , and  $g_\Delta$ . The masses and couplings are all running parameters that depend on the renormalization scale  $\Lambda$  and each of them satisfies a renormalization group equation. These equations and their solutions i.e. the running parameters were derived in Ref. [18]. The running masses and couplings can be used to obtain an RG-improved effective potential.

## B. Chemical potentials and neutrality conditions

According to Noether's theorem, there is one conserved charge for each continuous symmetry of the system. In principle, one can introduce an independent chemical potential  $\mu_i$  for each conserved charge  $Q_i$ . The corresponding number density is denoted by  $n_{Q_i}$ . However, this can only be done if the charges commute. In other words, we can introduce a maximum of  $N$  independent chemical potentials corresponding to the maximum number  $N$  of commuting charges of the system. In the present case, these are the baryon chemical potential  $\mu_B$ , the chemical potential for electric charge  $\mu_e$ , and the chemical potentials for the color charges  $Q_3$  and  $Q_8$ ,  $\mu_3$  and  $\mu_8$ . The pairing of quarks in the 2SC phase gives rise to a non-zero color charge  $Q_8$  in the ground state, while  $Q_3 = 0$ . Therefore, it is sufficient to introduce  $\mu_8$ . This is in contrast to the CFL phase of three-flavor QCD, where the ground state completely breaks the  $SU(3)_c$  symmetry. For this reason, both  $\mu_3$  and  $\mu_8$  must be introduced in order to impose color charge neutrality.

The quark chemical potential matrix can be expressed in terms of  $\mu_B$ ,  $\mu_e$ , and  $\mu_8$  as

$$\mu_{ij,\alpha\beta} = \left(\frac{1}{3}\mu_B\delta_{ij} - \mu_e Q_{ij}\right)\delta_{\alpha\beta} + \delta_{ij}\frac{2}{\sqrt{3}}\mu_8(T_8)_{\alpha\beta}, \quad (5)$$

where  $i, j$  are flavor indices and  $\alpha, \beta$  are color indices, and  $Q_{ij}$  are the matrix elements of the matrix  $Q = \text{diag}(\frac{2}{3}, -\frac{1}{3})$ . Alternatively, one could use the chemical potentials  $\mu_B$  and  $\mu_I$  instead with the replacement  $(\frac{1}{3}\mu_B\delta_{ij} - \mu_e Q_{ij}) \rightarrow (\frac{1}{3}\mu_B\delta_{ij} + \frac{1}{2}\mu_I I_{ij})\delta_{\alpha\beta}$  and  $I = \text{diag}(1, -1)$ . The expressions for the different quark chemical potentials follow from Eq. (5) as

$$\mu_{ur} = \mu_{ug} = \mu - \frac{2}{3}\mu_e + \frac{1}{3}\mu_8, \quad (6)$$

$$\mu_{dr} = \mu_{dg} = \mu + \frac{1}{3}\mu_e + \frac{1}{3}\mu_8, \quad (7)$$

$$\mu_{ub} = \mu - \frac{2}{3}\mu_e - \frac{2}{3}\mu_8, \quad (8)$$

$$\mu_{db} = \mu + \frac{1}{3}\mu_e - \frac{2}{3}\mu_8, \quad (9)$$

where  $\mu = \frac{1}{3}\mu_B$  is the common quark chemical potential. The number densities are given by

$$n_B = -\frac{\partial\Omega}{\partial\mu_B}, \quad (10)$$

$$n_e = -\frac{\partial\Omega}{\partial\mu_e}, \quad (11)$$

$$n_8 = -\frac{\partial\Omega}{\partial\mu_8}, \quad (12)$$

where  $\Omega$  is the thermodynamic potential. For arbitrary values of  $\mu_B$ ,  $\mu_e$ , and  $\mu_8$ , the electric charge density is non-zero,  $n_e \neq 0$ . However, a macroscopic chunk of quark matter must be electrically neutral, otherwise a huge energy price has to be paid due to the Coulomb interaction [19]. We therefore impose local electric charge neutrality on the system. The same remarks apply to the color charge  $Q_8$  and we therefore impose the two constraints

$$\frac{\partial\Omega}{\partial\mu_e} = \frac{\partial\Omega}{\partial\mu_8} = 0, \quad (13)$$

which finally leaves us with a single independent chemical potential, e. g.  $\mu_B$ . Electric charge neutrality is obtained by adding an electron background, which is achieved by adding the following term to the thermodynamic potential

$$\Omega_e = -\frac{4\mu_e^4}{3(4\pi)^2}. \quad (14)$$

In nature,  $U(1)_Q$  and  $SU(3)_c$  are local symmetries, and the zeroth components of the gauge fields serve as chemical potentials. The values of these fields are dynamically driven to values that set these charges to zero [20, 21]. In the quark-meson diquark model, the above-mentioned symmetries are global, and the chemical potentials must be introduced by hand. In normal quark matter, it is straightforward to derive that  $\mu_8 = 0$  guarantees color charge neutrality. However, in two-flavor QCD, normal quark matter is electrically charged since the trace of the electric charge matrix is non-zero. This requires a non-zero  $\mu_e$  and the presence of electrons. In the 2SC phase, electric and charge color neutrality is ensured by non-zero values of both  $\mu_e$  and  $\mu_8$ , as we shall see below.

## C. Quark spectrum and thermodynamic potential in the 2SC phase

We write the sigma  $\sigma$  and diquark field  $\Delta_3$  as a sum of their expectation values  $\phi_0$  and  $\Delta_0$ , and quantum fluctuating fields. This is done by making the substitutions

$$\sigma \rightarrow \phi_0 + \sigma, \quad (15)$$

$$\Delta_3 \rightarrow \Delta_0 + \Delta_3, \quad (16)$$

in the Lagrangian. Choosing  $\Delta_0$  real, the resulting tree-level thermodynamic potential is

$$\Omega_0 = \frac{1}{2}m^2\phi_0^2 + (m_\Delta^2 - 4\bar{\mu}^2)\Delta_0^2 + \frac{\lambda}{24}\phi_0^4 + \frac{\lambda_3}{12}\phi_0^2\Delta_0^2 + \frac{\lambda_\Delta}{6}\Delta_0^4 - h\phi_0, \quad (17)$$

where  $\bar{\mu}$  is defined in Eq. (25) below. The bilinear quark terms in the Lagrangian are

$$\mathcal{L}_{\text{bilinear}} = \bar{\psi}[i\not{\partial} - g\phi_0 + \hat{\mu}\gamma^0]\psi + \frac{1}{2}g_\Delta\bar{\psi}_b^C\Delta_0\gamma^5\tau_2\epsilon_{ab3}\psi_c + \frac{1}{2}g_\Delta\bar{\psi}_b\Delta_0^\dagger\gamma^5\tau_2\epsilon_{ab3}\psi_c^C. \quad (18)$$

Using the Nambu-Gorkov basis,  $\Psi = (\psi, \psi^C)$ , we then find the following inverse quark propagator

$$D^{-1}(p) = \begin{pmatrix} \not{p} - g\phi_0 + \gamma^0\hat{\mu} & ig_\Delta\tau_2\lambda_2\gamma^5\Delta_0 \\ ig_\Delta\tau_2\lambda_2\gamma^5\Delta_0 & \not{p} - g\phi_0 - \gamma^0\hat{\mu} \end{pmatrix}. \quad (19)$$

The zeros of the determinant of  $D^{-1}(p)$  give the fermion spectrum. We group the spectrum into the spectrum for the blue quarks

$$E_{ub}^\pm = E \pm \mu_{ub}, \quad (20)$$

$$E_{db}^\pm = E \pm \mu_{db}, \quad (21)$$

and the spectrum for the red and green quarks

$$E_{\Delta^\pm}^\pm = E_\Delta^\pm \pm \delta\mu, \quad (22)$$

where the energies and chemical potentials are defined as

$$E = \sqrt{p^2 + g^2\phi_0^2}, \quad (23)$$

$$E_\Delta^\pm = \sqrt{(E \pm \bar{\mu})^2 + g_\Delta^2\Delta_0^2}, \quad (24)$$

$$\bar{\mu} = \frac{1}{2}(\mu_{ur} + \mu_{dg}) = \frac{1}{2}(\mu_{ug} + \mu_{dr}) = \mu - \frac{1}{6}\mu_e + \frac{1}{3}\mu_s, \quad (25)$$

$$\delta\mu = \frac{1}{2}(\mu_{dg} - \mu_{ur}) = \frac{1}{2}(\mu_{dr} - \mu_{ug}) = \frac{1}{2}\mu_e, \quad (26)$$

The chemical potential  $\delta\mu$  is referred to as the mismatch parameter since it measures the mismatch between the Fermi surfaces of the  $u$  and the  $d$  quarks, i.e. the quarks that form pairs. A large value  $\delta\mu$  disfavors Cooper pairing as we shall see below. The ungapped quasiparticles Eqs. (20)–(21) are singlets under the unbroken  $SU(2)_c$  symmetry, each with a degeneracy factor one. The quasiparticles in Eq. (22) form two doublets under the unbroken  $SU(2)_c$  symmetry, each with a degeneracy factor of two. This gives a total of six quark and six antiquark quasiparticles. They become degenerate when the mismatch parameter vanishes. The doublet with energy  $E_{\Delta^+}^-$  has a gap  $\Delta_0 + \delta\mu$ , while the doublet with energy  $E_{\Delta^-}^-$  has a gap  $\Delta_0 - \delta\mu$  as long as  $\delta\mu < \Delta_0$ . When  $\delta\mu \geq \Delta_0$ , this mode becomes gapless and the corresponding phase is referred to as the gapless 2SC phase (g2SC) [22].

We now turn to the thermodynamic potential  $\Omega$ . We work in the approximation, where bosons are treated at tree level, whereas we include Gaussian fluctuations of the quarks. The one-loop contribution to the thermodynamic potential from the quarks is

$$\Omega_1 = -2 \int_p \left\{ 2E + T \log \left[ 1 + e^{-\beta E_{ub}^\pm} \right] + T \log \left[ 1 + e^{-\beta E_{db}^\pm} \right] \right\} - 4 \int_p \left\{ E_\Delta^\pm + T \log \left[ 1 + e^{-\beta E_{\Delta^\pm}^\pm} \right] \right\}, \quad (27)$$

which is added to the tree-level term Eq. (17). The integrals  $\int_p$  are defined in  $d = 3 - 2\epsilon$  dimension as

$$\int_p = \left( \frac{e^{\gamma_E} \Lambda^2}{4\pi} \right)^\epsilon \int \frac{d^d p}{(2\pi)^d}, \quad (28)$$

where  $\Lambda$  is the renormalization scale associated with the  $\overline{\text{MS}}$ -scheme. The final result for the thermodynamic potential

at  $T = 0$ , including quark loops was derived in Ref. [18] and reads

$$\begin{aligned}
\Omega_{0+1} = & \frac{3}{4} m_\pi^2 f_\pi^2 \left\{ 1 - \frac{12m_q^2}{(4\pi)^2 f_\pi^2} m_\pi^2 F'(m_\pi^2) \right\} \frac{\phi_0^2}{f_\pi^2} + \frac{2m_q^4}{(4\pi)^2} \left( \frac{9}{2} + \log \frac{m_q^2}{g_0^2 \phi_0^2} + 2 \log \frac{m_q^2}{g_0^2 \phi_0^2 + g_{\Delta,0}^2 \Delta_0^2} \right) \frac{\phi_0^4}{f_\pi^4} \\
& - \frac{1}{4} m_\sigma^2 f_\pi^2 \left\{ 1 + \frac{12m_q^2}{(4\pi)^2 f_\pi^2} \left[ \left( 1 - \frac{4m_q^2}{m_\sigma^2} \right) F(m_\sigma^2) + \frac{4m_q^2}{m_\sigma^2} - F(m_\pi^2) - m_\pi^2 F'(m_\pi^2) \right] \right\} \frac{\phi_0^2}{f_\pi^2} \\
& + \frac{1}{8} m_\sigma^2 f_\pi^2 \left\{ 1 + \frac{12m_q^2}{(4\pi)^2 f_\pi^2} \left[ \left( 1 - \frac{4m_q^2}{m_\sigma^2} \right) F(m_\sigma^2) - F(m_\pi^2) - m_\pi^2 F'(m_\pi^2) \right] \right\} \frac{\phi_0^4}{f_\pi^4} \\
& - \frac{1}{8} m_\pi^2 f_\pi^2 \left\{ 1 - \frac{12m_q^2}{(4\pi)^2 f_\pi^2} m_\pi^2 F'(m_\pi^2) \right\} \frac{\phi_0^4}{f_\pi^4} - m_\pi^2 f_\pi^2 \left\{ 1 - \frac{12m_q^2}{(4\pi)^2 f_\pi^2} m_\pi^2 F'(m_\pi^2) \right\} \frac{\phi_0}{f_\pi} \\
& + \left\{ m_{\Delta,0}^2 - 4\bar{\mu}^2 \left[ 1 + \frac{4g_{\Delta,0}^2}{(4\pi)^2} \left( \log \frac{m_q^2}{g_0^2 \phi_0^2 + g_{\Delta,0}^2 \Delta_0^2} - F(m_\pi^2) - m_\pi^2 F'(m_\pi^2) \right) \right] \right\} \Delta_0^2 \\
& + \frac{\lambda_{3,0}}{12} \phi_0^2 \Delta_0^2 + \frac{\lambda_{\Delta,0}}{6} \Delta_0^4 + \frac{12g_0^2 g_{\Delta,0}^2}{(4\pi)^2} \phi_0^2 \Delta_0^2 + \frac{6g_{\Delta,0}^4}{(4\pi)^2} \Delta_0^4 \\
& + \frac{4g_{\Delta,0}^4}{(4\pi)^2} \left\{ \log \frac{m_q^2}{g_0^2 \phi_0^2 + g_{\Delta,0}^2 \Delta_0^2} - F(m_\pi^2) - m_\pi^2 F'(m_\pi^2) \right\} \Delta_0^4 \\
& + \frac{8g_0^2 g_{\Delta,0}^2}{(4\pi)^2} \left\{ \log \frac{m_q^2}{g_0^2 \phi_0^2 + g_{\Delta,0}^2 \Delta_0^2} - F(m_\pi^2) - m_\pi^2 F'(m_\pi^2) \right\} \phi_0^2 \Delta_0^2 + \Omega_1^{\text{fin}} + \Omega_1^\mu, \tag{29}
\end{aligned}$$

where  $g_{\Delta,0}^2$  and  $\Delta_0^2$  are the running coupling and field  $g_{\Delta,\overline{\text{MS}}}^2$  and  $\Delta_{\overline{\text{MS}}}^2$  evaluated at a reference scale, but the product  $g_{\Delta,\overline{\text{MS}}}^2 \Delta_{\overline{\text{MS}}}^2$  is scale invariant. The same remark applies to  $g_0^2$  and  $\phi_0^2$ . Moreover, the function  $F(p^2) = 2 - 2q \arctan(\frac{1}{q})$  with  $q = \sqrt{\frac{4m_q^2}{p^2} - 1}$ , and

$$\Omega_1^{\text{fin}} = -4\Lambda^{-2\epsilon} \int_p \left[ E_{\Delta^\pm}^\pm - 2\sqrt{p^2 + g^2 \phi_0^2 + g_\Delta^2 \Delta_0^2} - \frac{\bar{\mu}^2 g_\Delta^2 \Delta_0^2}{(p^2 + g^2 \phi_0^2 + g_\Delta^2 \Delta_0^2)^{\frac{3}{2}}} \right], \tag{30}$$

$$\Omega_1^\mu = 2\Lambda^{-2\epsilon} \int_p [(E \mp \mu_{ub})\theta(\pm\mu_{ub} - E) + (E \mp \mu_{db})\theta(\pm\mu_{db} - E) + 2(E_\Delta^\pm \mp \delta\mu)\theta(\pm\delta\mu - E_\Delta^\pm)]. \tag{31}$$

Note that the integrals in Eqs. (30)–(31) are finite in  $d = 3$ .

#### D. Nambu-Goldstone bosons in the 2SC phase

The formation of Cooper pairs and the resulting non-zero gap  $\Delta_0$  in the 2SC phase break the  $SU(3)_c$  symmetry down to  $SU(2)_c$ . In QCD with dynamical gluons, there is no breaking of the local  $SU(3)_c$  symmetry, however, and the gap  $\Delta_0$  is a gauge-variant quantity. Only the magnitude  $|\Delta_0|$  is gauge invariant. Instead of a number of NG modes in the physical spectrum, the Higgs mechanism leads to five massive gluons, one for each broken generator [23]. In the QMD model, the  $SU(3)_c$  symmetry is global and its breaking to  $SU(2)_c$  should naively lead to five massless excitations, or Nambu-Goldstone bosons,

corresponding to the five broken generators.<sup>2</sup> Naively, since it is only in Lorentz-invariant theories that Goldstone's theorem guarantees that the number of massless excitations equals the number of broken generators. Starting with the paper by Chadha and Nielsen [25], there has been significant progress in the classification of Nambu-Goldstone bosons and their properties; see e.g. [26–29], and [30] for a comprehensive review.

The complex antitriplet  $\Delta_a$  can be parametrized in terms of six real fields. In order to simplify the discussion and obtain analytical results, we set  $\phi_0 = 0$  in the remainder of this section. There is no loss of generality since the symmetry-breaking pattern in the diquark sector remains the same  $SU(3)_c \rightarrow SU(2)_c$ . Writing

<sup>2</sup> The NG boson have been discussed in the context of the NJL model in Ref. [24]. In the NJL model, the NG modes are propagating only after taking quark loops into account.

$\Delta_3 = \Delta_0 + \Delta_3 = \Delta_0 + \frac{1}{\sqrt{2}}(\phi_1 + i\phi_2)$  and using a common quark chemical potential  $\mu$ , the relevant terms up to quadratic order are

$$\begin{aligned} \mathcal{L}_{\text{quad}}^{\text{bosons}} &= (\partial_\mu + 2i\delta_{\mu 0}\mu)\Delta_1^\dagger(\partial_\mu - 2i\delta_{\mu 0}\mu)\Delta_1 \\ &\quad - (m_\Delta^2 + \frac{\lambda_\Delta}{3}\Delta_0^2)\Delta_1^\dagger\Delta_1 \\ &\quad + (\partial_\mu + 2i\delta_{\mu 0}\mu)\Delta_2^\dagger(\partial_\mu - 2i\delta_{\mu 0}\mu)\Delta_2 \\ &\quad - (m_\Delta^2 + \frac{\lambda_\Delta}{3}\Delta_0^2)\Delta_2^\dagger\Delta_2 \\ &\quad + \frac{1}{2}(\partial_\mu\phi_1)(\partial^\mu\phi_1) - \frac{1}{2}(m_\Delta^2 - 4\mu^2 + \lambda_\Delta\Delta_0^2)\phi_1^2 \\ &\quad + \frac{1}{2}(\partial_\mu\phi_2)(\partial^\mu\phi_2) - \frac{1}{2}(m_\Delta^2 - 4\mu^2 + \frac{\lambda_\Delta}{3}\Delta_0^2)\phi_2^2 \\ &\quad + 2\mu(\partial_0\phi_1\phi_2 - \partial_0\phi_2\phi_1), \end{aligned} \quad (32)$$

The spectrum is found by calculating the zeros of the determinant of the propagator in the usual way. Note that we need to evaluate the diquark field  $\Delta_0$  at the minimum (on shell) of the tree-level thermodynamic potential  $\Omega_0$ , i.e. for  $(m_\Delta^2 - 4\mu^2)\Delta_0 + \frac{\lambda_\Delta}{3}\Delta_0^3 = 0$ . This yields the dispersion relations

$$E_{\Delta_1}^\pm = \sqrt{p^2 + 4\mu^2} \pm 2\mu, \quad (33)$$

$$E_{\Delta_2}^\pm = \sqrt{p^2 + 4\mu^2} \pm 2\mu, \quad (34)$$

$$E_{\Delta_3}^\pm = \sqrt{p^2 + 12\mu^2 - m_\Delta^2} \pm \sqrt{16p^2\mu^2 + (12\mu^2 - m_\Delta^2)^2}. \quad (35)$$

The massless NG modes in Eqs. (33)–(34) are quadratic for small momenta  $p$ , while the massless NG mode in Eq. (35) is linear for small momenta. Linear modes are referred to as type A and quadratic modes as type B. Moreover, the partners of the type-B NG modes are massive with mass  $4\mu$ .

A counting rule for the numbers of type-A and type-B NG modes has been derived in Refs. [26, 27]. Denoting these numbers by  $n_A$  and  $n_B$ , respectively, the rule is

$$n_A = \dim G - \dim H - \text{rank } \varrho, \quad (36)$$

$$n_B = \frac{1}{2}\text{rank } \varrho, \quad (37)$$

where  $G$  is the full symmetry group,  $H$  is the unbroken subgroup, and  $\varrho$  is the commutator matrix with matrix elements

$$\varrho_{ab} = \lim_{V \rightarrow \infty} \frac{i}{V} \langle 0|[T_a, T_b]|0 \rangle, \quad (38)$$

where  $\langle 0|A|0 \rangle$  is the ground-state expectation value of  $A$ , and  $V$  is the spatial volume of the system. It is clear that  $\varrho_{ab} = 0$  whenever the generators  $T_a$  and  $T_b$  are unbroken. In the present case,  $G = SU(3)_c$  and  $H = SU(2)_c$ . The only non-zero matrix elements are  $\varrho_{45} = -\varrho_{54} = i\langle [T_4, T_5] \rangle$  and  $\varrho_{67} = -\varrho_{76} = i\langle [T_6, T_7] \rangle$ . This yields  $\text{rank } \varrho = 4$ , and therefore  $n_A = 1$  and  $n_B = 2$ ,

in accordance with our explicit calculations. The commutators  $[T_a, T_b]$  can be written as a linear combination of the symmetry generators  $T_3$  and  $T_8$ . Thus, if color charge neutrality is enforced in the 2SC phase,  $Q_8 = 0$ , Eq. (38) immediately yields  $\varrho = 0$ , and therefore the number of type-A NG bosons,  $n_A$ , equals the number of broken generators, as first shown in Ref. [31]. In the present case, there are five NG bosons with a linear dispersion relation for small momenta  $p$ . The massive modes in Eqs. (33)–(34) are also special in the sense that their gap is determined by symmetry [32]. Their number is given by the number of pairs of broken generators  $T_a$  that do not commute with  $T_8$ . There are two such pairs,  $T_4 \pm iT_5$  and  $T_6 \pm iT_7$ , which leads to two massive NG bosons. Finally, as pointed out in Ref. [33], the NG bosons do not Bose condense in the 2SC phase. Condensation corresponds to a change of the relative flavor orientation of the left and right-handed condensates. Since these condensates are singlets under  $SU(2)_L \times SU(2)_R$  this cannot happen. This is in contrast to NG bosons in the CFL phase in three-flavor QCD [11].

### E. Pion condensation at finite isospin $\mu_I$

In this section, we will discuss charged pion condensation at finite isospin chemical potential and zero baryon chemical potential. The onset of pion condensation at  $T = 0$  is a second-order transition that takes place exactly at the pion mass,  $\mu_I = m_\pi$ . As mentioned in the Introduction, QCD is amenable to lattice simulations for  $\mu_B = 0$ , since the sign problem is absent in this case.

Chiral perturbation theory [5, 6] provides a systematic low-energy expansion of the chiral Lagrangian based on the symmetries and degrees of freedom of QCD, and gives model-independent predictions. At finite  $\mu_I$ , the expansion parameters are  $m_\pi^2/(4\pi)^2 f_\pi^2$  and  $\mu_I^2/(4\pi)^2 f_\pi^2$ . For sufficiently small values of  $\mu_I$ , we can therefore use chiral perturbation theory to describe the BEC phase. The tree-level expressions for the pressure and the energy density in the pion-condensed phase are the same for two and three-flavor QCD, and given by [4]

$$p = \frac{1}{2}f_\pi^2\mu_I^2 \left[ 1 - \frac{m_\pi^2}{\mu_I^2} \right]^2, \quad m_\pi \leq \mu_I, \quad (39)$$

$$\epsilon(p) = -p + 2\sqrt{p(p + 2f_\pi^2 m_\pi^2)}. \quad (40)$$

In the vacuum phase, which extends from  $\mu_I = 0$  to  $\mu_I = m_\pi$ , the pressure and energy density vanish identically,  $p = \epsilon = c_s^2 = 0$ . From the expressions, one can find the speed of sound squared, expressed in terms of the pion mass and the isospin chemical potential,

$$c_s^2 = \frac{dp}{d\epsilon} = \frac{\mu_I^4 - m_\pi^4}{\mu_I^4 + 3m_\pi^4}. \quad (41)$$

The speed of sound is zero in the vacuum phase and approaches unity in the ultra-relativistic limit  $\mu_I \rightarrow \infty$ .

The large- $\mu_I$  behavior is due to the fact that the pressure is proportional to  $\mu_I^2$  and consequently the equation of state becomes  $\epsilon = p$  at large  $\mu_I$ . However,  $\chi$ PT is not valid for large values of the isospin chemical potential. We can get an idea of the convergence properties of  $\chi$ PT at finite  $\mu_I$  by comparing the predictions for different physical quantities at LO and NLO order. A conservative estimate suggests that  $\chi$ PT is reliable for  $\mu_I$  up to 200 MeV [10]. The behavior at large  $\mu_I$  is in disagreement with the conformal limit of QCD, where  $c_s^2 = \frac{1}{3}$ . The reason is that pions are not the correct degrees of freedom at high (isospin) density. In this region, one should rather think in terms of a Fermi surface that is rendered unstable due to an attractive interaction channel and the formation of loosely bound Cooper pairs of  $u$  and  $\bar{d}$  quarks. Since Cooper pairs have the same quantum

numbers as the pion, one expects a crossover rather than a phase transition. This is called the BEC-BCS crossover. We will not focus on this crossover, but simply refer to this part of the phase diagram as the BEC/BCS phase.

The quark-meson model has also been used as a low-energy model to study QCD at finite isospin [34–41]. Denoting the pion condensate by  $\rho_0$ , the tree-level thermodynamic potential is

$$\Omega_0 = \frac{1}{2}m^2\phi_0^2 + \frac{1}{2}(m^2 - \mu_I^2)\rho_0^2 + \frac{\lambda}{24}(\phi_0^2 + \rho_0^2)^2 - h\phi_0. \quad (42)$$

The one-loop thermodynamic potential with on-shell renormalization was derived in Ref. [36] for  $N_c$  colors, and we give it here for completeness,

$$\begin{aligned} \Omega_{0+1} = & \frac{3}{4}m_\pi^2 f_\pi^2 \left\{ 1 - \frac{4m_q^2 N_c}{(4\pi)^2 f_\pi^2} m_\pi^2 F'(m_\pi^2) \right\} \frac{\phi_0^2 + \rho_0^2}{f_\pi^2} \\ & - \frac{1}{4}m_\sigma^2 f_\pi^2 \left\{ 1 + \frac{4m_q^2 N_c}{(4\pi)^2 f_\pi^2} \left[ \left(1 - \frac{4m_q^2}{m_\sigma^2}\right) F(m_\sigma^2) + \frac{4m_q^2}{m_\sigma^2} - F(m_\pi^2) - m_\pi^2 F'(m_\pi^2) \right] \right\} \frac{\phi_0^2 + \rho_0^2}{f_\pi^2} \\ & - \frac{1}{2}\mu_I^2 f_\pi^2 \left\{ 1 - \frac{4m_q^2 N_c}{(4\pi)^2 f_\pi^2} \left[ \log \frac{\phi_0^2 + \rho_0^2}{f_\pi^2} + F(m_\pi^2) + m_\pi^2 F'(m_\pi^2) \right] \right\} \frac{\rho_0^2}{f_\pi^2} \\ & + \frac{1}{8}m_\sigma^2 f_\pi^2 \left\{ 1 - \frac{4m_q^2 N_c}{(4\pi)^2 f_\pi^2} \left[ \frac{4m_q^2}{m_\sigma^2} \left( \log \frac{\phi_0^2 + \rho_0^2}{f_\pi^2} - \frac{3}{2} \right) - \left(1 - \frac{4m_q^2}{m_\sigma^2}\right) F(m_\sigma^2) + F(m_\pi^2) + m_\pi^2 F'(m_\pi^2) \right] \right\} \frac{(\phi_0^2 + \rho_0^2)^2}{f_\pi^4} \\ & - \frac{1}{8}m_\pi^2 f_\pi^2 \left[ 1 - \frac{4m_q^2 N_c}{(4\pi)^2 f_\pi^2} m_\pi^2 F'(m_\pi^2) \right] \frac{(\phi_0^2 + \rho_0^2)^2}{f_\pi^4} - m_\pi^2 f_\pi^2 \left[ 1 - \frac{4m_q^2 N_c}{(4\pi)^2 f_\pi^2} m_\pi^2 F'(m_\pi^2) \right] \frac{\phi_0}{f_\pi} + \Omega_1^{\text{fin}} + \Omega_1^\mu, \quad (43) \end{aligned}$$

where  $\rho_0^2 = \rho_{0,\overline{\text{MS}}}^2$  at a reference scale, with  $g_0^2 \rho_0^2 = g_{0,\overline{\text{MS}}}^2 \rho_{0,\overline{\text{MS}}}^2$  being scale invariant, and

$$\Omega_1^{\text{fin}} = -2N_c \Lambda^{-2\epsilon} \int_p \left[ E_{\rho_0}^\pm - 2\sqrt{p^2 + g_0^2(\phi_0^2 + \rho_0^2)} - \frac{\mu_I^2 \rho_0^2}{4[p^2 + g_0^2(\phi_0^2 + \rho_0^2)]^{\frac{3}{2}}} \right], \quad (44)$$

$$\Omega_1^\mu = 2N_c \Lambda^{-2\epsilon} \int_p \left[ (E_{\rho_0}^\pm - \mu)\theta(\mu - E_{\rho_0}^\pm) + (E_{\rho_0}^\pm + \mu)\theta(-\mu - E_{\rho_0}^\pm) \right]. \quad (45)$$

Here the fermionic quasiparticle spectrum is

$$E_{\rho_0}^\pm = \sqrt{(E \pm \frac{1}{2}\mu_I)^2 + g_0^2 \rho_0^2}, \quad (46)$$

with  $E = \sqrt{p^2 + g_0^2 \phi_0^2}$ . Note the similarity between the gapped spectra Eq. (22) and Eq. (46) for  $\delta\mu = 0$ . The integral Eqs. (44) is evaluated numerically directly in  $d =$

3 dimensions. Eqs. (29) and (43) is the starting point for mapping out the phase diagram.

### F. Behavior at large chemical potentials

For large chemical potentials  $\mu$  or  $\mu_I$ , we can obtain simple expressions for thermodynamic quantities such as pressure and energy density. We first consider large  $\mu$ .

If we are deep in the 2SC phase, we have  $\phi_0 \ll \Delta_0$ . The thermodynamical potential in Eq. (29) reduces to

$$\begin{aligned} \Omega_{0+1} = & (m_{\Delta,0}^2 - 4\bar{\mu}^2)\Delta_0^2 + \frac{\lambda_{\Delta,0}}{6}\Delta_0^4 - \frac{4(4\bar{\mu}^4 + \mu_{ub}^4 + \mu_{db}^4)}{3(4\pi)^2} - \frac{16g_{\Delta,0}^2}{(4\pi)^2} \left[ \log \frac{m_q^2}{g_{\Delta,0}^2 \Delta_0^2} - F(m_\pi^2) - m_\pi^2 F'(m_\pi^2) \right] \bar{\mu}^2 \Delta_0^2 \\ & + \frac{4g_{\Delta,0}^4}{(4\pi)^2} \left[ \log \frac{m_q^2}{g_{\Delta,0}^2 \Delta_0^2} + \frac{3}{2} - F(m_\pi^2) - m_\pi^2 F'(m_\pi^2) \right] \Delta_0^4. \quad (47) \end{aligned}$$

In the same approximation, the gap equation reads

$$0 = m_{\Delta,0}^2 - 4\bar{\mu}^2 + \frac{\lambda_{\Delta,0}}{3}\Delta_0^2 - \frac{16g_{\Delta,0}^2}{(4\pi)^2} \left[ \log \frac{m_q^2}{g_{\Delta,0}^2\Delta_0^2} - 1 - F(m_\pi^2) - m_\pi^2 F'(m_\pi^2) \right] \bar{\mu}^2 + \frac{8g_{\Delta,0}^4}{(4\pi)^2} \left[ \log \frac{m_q^2}{g_{\Delta,0}^2\Delta_0^2} + 1 - F(m_\pi^2) - m_\pi^2 F'(m_\pi^2) \right] \Delta_0^2. \quad (48)$$

Assuming  $\bar{\mu} \gg \Delta_0$ , we can solve the gap equation explicitly. Denoting  $\Delta_0$  by  $\bar{\Delta}_0$  in this regime, we find

$$\bar{\Delta}_0^2 = \frac{m_q^2}{g_{\Delta,0}^2} \exp \left[ \frac{(4\pi)^2}{4g_{\Delta,0}^2} - 1 - F(m_\pi^2) - m_\pi^2 F'(m_\pi^2) \right] \quad (49)$$

In other words, the gap  $g_{\Delta,0}\bar{\Delta}_0$  approaches a constant as  $\bar{\mu} \rightarrow \infty$ . This is in contrast to the behavior of the gap at tree-level. In this case, the gap increases linearly with  $\bar{\mu}$ . The difference is caused by the logarithms introduced by adding quark loops. Note that the gap  $g_{\Delta,0}\bar{\Delta}_0$  depends only on the diquark coupling  $g_{\Delta,0}$  and the zero-temperature quark mass  $m_q$ . In principle, we can use the result Eq. (49) to connect to perturbative QCD. We simply tune the parameter so that it agrees with the gap calculated in pQCD for a given large value of  $\mu$ .<sup>3</sup>

The pressure  $p$  is given by minus the thermodynamic potential  $\Omega_{0+1}$ , evaluated at the solution of the gap equation. At high densities, the pressure reduces to

$$p = \frac{4(4\bar{\mu}^4 + \mu_{ub}^4 + \mu_{db}^4)}{3(4\pi)^2} + \frac{16\bar{\mu}^2 g_{\Delta,0}^2 \bar{\Delta}_0^2}{(4\pi)^2} + \frac{4\mu_e^4}{3(4\pi)^2} \quad (50)$$

Except for the term  $\frac{4(\mu_{sr}^4 + \mu_{sg}^4 + \mu_{sb}^4)}{3(4\pi)^2}$  coming from unpaired  $s$  quarks, the result for the pressure Eq. (50) is the same as obtained for the 2SC phase in the three-flavor case based on an analytic approximation of the NJL model [42].<sup>4</sup> The corrections to the pressure due to the color superconductivity are parametrically suppressed by  $\bar{\Delta}_0^2/\bar{\mu}^2$ , which can be understood as follows. Whereas Cooper pairing affects only states close to the Fermi surface, the Pauli pressure receives contributions from the entire Fermi sphere. The energy density  $\epsilon$  and trace anomaly  $\langle T_\alpha^\alpha \rangle$  are given by

$$\epsilon = \frac{4(4\bar{\mu}^4 + \mu_{ub}^4 + \mu_{db}^4)}{(4\pi)^2} + \frac{16\bar{\mu}^2 g_{\Delta,0}^2 \bar{\Delta}_0^2}{(4\pi)^2} + \frac{4\mu_e^4}{(4\pi)^2} \quad (51)$$

$$\langle T_\alpha^\alpha \rangle = -\frac{32\bar{\mu}^2 g_{\Delta,0}^2 \bar{\Delta}_0^2}{(4\pi)^2}. \quad (52)$$

Comparing Eqs. (29) and (43), we note that the expressions for the thermodynamic potential are essentially the

same, the one-loop terms differ by numerical factors and the relevant couplings. This implies that the gap, pressure, energy density, trace anomaly, and speed of sound have the same behavior at large  $\mu_I$ . As in the 2SC phase, we calculate the thermodynamic potential deep into the BCS phase using  $\phi_0 \approx 0$ . This yields

$$\bar{\rho}_0^2 = \frac{m_q^2}{g_0^2} \exp \left[ \frac{(4\pi)^2}{4N_c g_0^2} - 1 - F(m_\pi^2) - m_\pi^2 F'(m_\pi^2) \right] \quad (53)$$

$$p = \frac{N_c \mu_I^4}{6(4\pi)^2} + \frac{2N_c \mu_I^2 g_0^2 \bar{\rho}_0^2}{(4\pi)^2}, \quad (54)$$

$$\epsilon = \frac{N_c \mu_I^4}{2(4\pi)^2} + \frac{2N_c \mu_I^2 g_0^2 \bar{\rho}_0^2}{(4\pi)^2}, \quad (55)$$

$$\langle T_\alpha^\alpha \rangle = -\frac{4N_c \mu_I^2 g_0^2 \bar{\rho}_0^2}{(4\pi)^2}, \quad (56)$$

In contrast to the superconducting gap, the asymptotic value of the pion condensate  $\bar{\rho}_0$  is completely determined by vacuum physics.

### III. RESULTS AND DISCUSSION

In this section, we discuss our numerical results. The values of the meson masses and the pion decay constant are

$$m_\pi = 140 \text{ MeV}, \quad (57)$$

$$m_\sigma = 600 \text{ MeV}, \quad (58)$$

$$f_\pi = 93 \text{ MeV}. \quad (59)$$

In addition, the quark mass is

$$m_q = 300 \text{ MeV}. \quad (60)$$

We also set  $N_c = 3$ . As we have explained, the remaining parameters are treated as free. A natural guess for the parameters would be  $g_\Delta \sim g$ ,  $\lambda \sim \lambda_3 \sim \lambda_\Delta$ , which in [18] was shown to yield reasonable results. It turns out that the results are sensitive mainly to the diquark mass parameter  $m_\Delta$  and the diquark coupling  $g_\Delta$ . The position of the transition to the 2SC phase depends on both parameters, while the gap is largely determined by the latter. To illustrate the possible phase diagrams, we have chosen two sets of parameters,

$$\text{set 1 : } \quad m_\Delta = 500 \text{ MeV}, \quad g_\Delta = 2g, \quad (61)$$

$$\text{set 2 : } \quad m_\Delta = 900 \text{ MeV}, \quad g_\Delta = 2g. \quad (62)$$

<sup>3</sup> We have to multiply by  $2^{-\frac{1}{3}}$  since the CFL gap is related to the 2SC gap by this factor [2].

<sup>4</sup> The chemical potentials  $\mu_{sr}$ ,  $\mu_{sg}$ , and  $\mu_{sb}$  are expressed in terms of  $\mu$ ,  $\mu_c$ ,  $\mu_8$  as well as the mass  $m_s$  of the  $s$  quark.



The first set is one of the four parameter sets used in our previous analysis in Ref. [18]. The second set was chosen to show that NQM is possible when neutrality has been imposed (see Fig. 4 below). We mentioned in Sec. II F that we can determine  $g_\Delta$  by equating our asymptotic value for the gap to the gap at large densities obtained from pQCD. We can also determine it from other constraints on the gap at large densities. Recently, [43] used astrophysical observations to obtain an upper bound on the CFL gap of 216 MeV at baryon chemical potential  $\mu_B = 2.6$  GeV. We therefore ensure that our gap does not exceed this limit  $g_\Delta \Delta_0 \leq 268 = 2^{-\frac{1}{3}} 216$  MeV for large  $\mu$ . More generally, the parameter with the largest effect is  $g_\Delta$ . Increasing  $g_\Delta$  leads to an earlier transition from vacuum or NQM to the 2SC phase. Increasing  $g_\Delta$  also leads to lower gap values. Constraining this parameter is therefore of most importance. In our analysis, for simplicity, we have fixed  $\tilde{\lambda} = \lambda_3 = \frac{1}{4}\lambda_\Delta$  and varied these parameters together. Increasing the parameter  $\tilde{\lambda}$  leads to a larger gap. Lastly, increasing (decreasing)  $m_\Delta$  leads to a later (earlier) transition to the 2SC phase, either from the vacuum or NQM.

To find the minimum of the thermodynamic potential  $\Omega_{0+1}$ , we must simultaneously solve the two gap equations

$$\frac{\partial \Omega_{0+1}}{\partial \phi_0} = \frac{\partial \Omega_{0+1}}{\partial \Delta_0} = 0, \quad (2SC) \quad (63)$$

$$\frac{\partial \Omega_{0+1}}{\partial \phi_0} = \frac{\partial \Omega_{0+1}}{\partial \rho_0} = 0, \quad (\text{BEC/BCS}) \quad (64)$$

using Eq. (29) and Eq. (43), respectively, and then choose the global minimum. Imposing electric charge and color charge neutrality, the Eqs. (13) and (64) are solved simultaneously.

In Fig. 1, we show the zero-temperature phase diagram in the  $\mu$ - $\mu_I$  plane using parameter set 1. The red line is the phase boundary between the pion-condensed phase and the vacuum phase or normal quark matter. The blue line is the phase boundary between the vacuum phase and either normal quark matter or the 2SC phase, whereas the green line is the phase boundary between NQM and the color superconducting phase.

In Fig. 2, we show the zero-temperature phase diagram in the  $\mu$ - $\mu_I$  plane using parameter set 2. The color coding is the same as in Fig. 1, but now normal quark matter exists in a much larger region in the plane. Below we shall see that this gives rise to electrically neutral normal quark matter.

In Fig. 3, we show the quark condensate (black line), superconducting gap (green line), the mismatch parameter  $\delta\mu = \frac{1}{2}\mu_e$  (blue line), and the color chemical potential  $\mu_8$  (red line) as functions of the quark chemical potential  $\mu$  for parameter set 1. For these parameters, the transition is directly from the vacuum to the 2SC phase. The chemical potentials vanish in the entire region up to the transition to the 2SC phase, which reflects that the vacuum state is neutral. Since the 2SC ground state carries both color and electric charge, both chemical potentials

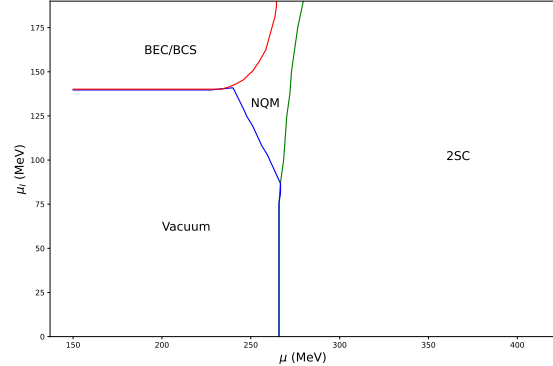


FIG. 1. Phase diagram in the  $\mu$ - $\mu_I$  plane at  $T = 0$  for parameters set 1. See main text for details.

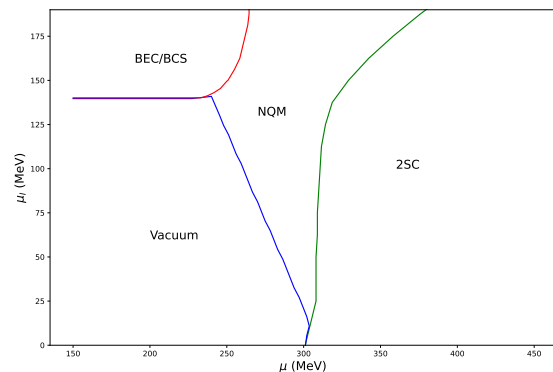


FIG. 2. Phase diagram in the  $\mu$ - $\mu_I$  plane at  $T = 0$  for parameters set 2. See main text for details.

$\mu_e$  and  $\mu_8$  are non-zero in order to satisfy the charge neutrality conditions. Note that the  $\delta\mu = \frac{1}{2}\mu_e > 0$  such that the electron density is positive, which is needed to neutralize the positively charged 2SC state. The superconducting gap grows as  $\mu$  increases approaches a constant for large values of the chemical potential, cf Eq. (49). This is in contrast to the NJL model, where the gap has a maximum at  $\mu \approx 500$  MeV, after which it drops rather quickly to zero. As pointed out in Ref. [44], this unphysical behavior is a regularization artifact.

In Fig. 4, we show the same quantities as in Fig. 3 but now for parameter set 2. The difference is that there is a phase of normal quark matter between the vacuum phase and the 2SC phase. Two-flavor normal quark matter is not electrically neutral without an electron background, which is why  $\delta\mu = \frac{1}{2}\mu_e$  (blue line) becomes non-zero before the superconducting gap (green line) and  $\mu_8$  (red line). For our two parameters sets, there is no transition to the g2SC phase since this requires that the  $\delta\mu$  given by the blue line lies above the gap  $\Delta_0$  given by the green line.

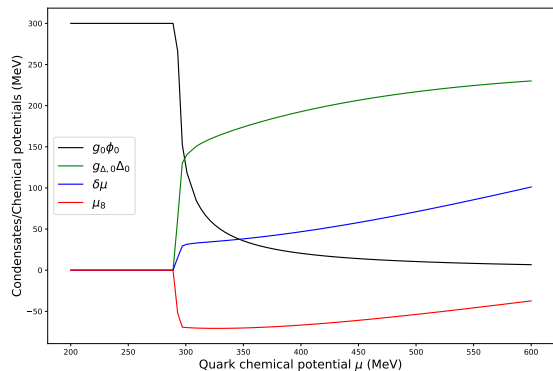


FIG. 3. Quark condensate (black line), superconducting gap (green line), mismatch parameter (blue line), and color chemical potential (red line) as functions of  $\mu$  for parameter set 1. See main text for details.

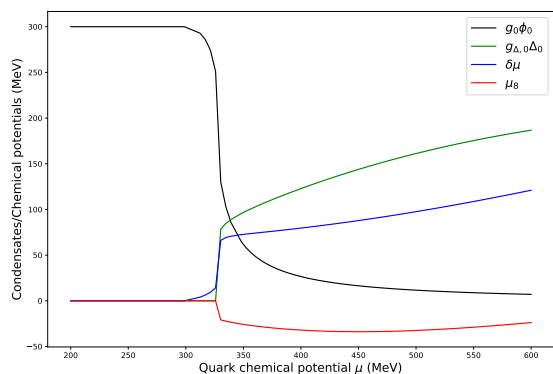


FIG. 4. Quark condensate (black line), superconducting gap (green line), mismatch parameter (blue line), and color chemical potential (red line) as functions of  $\mu$  for parameter set 2. See main text for details.

Next, we consider the speed of sound  $c_s$ , which is of interest because it gives information about the stiffness of the equation of state. The EoS is crucial in understanding the structure of neutron stars. Before we discuss the case of finite quark chemical potential, we consider finite isospin for which lattice data exist. For similar results and analysis, see Ref. [38] and very recently Ref. [41]. In Fig. 5, we show the result for the speed of sound squared  $c_s^2$  as a function of  $\mu_I/m_\pi$  using the quark-meson model (blue line). We also show the results for two-flavor leading-order (LO) and next-to-leading-order (NLO) chiral perturbation theory [10]. The green band is simply the region between the LO (upper line) and the NLO (lower line) results. Note that the blue curve lies entirely within this band. We also show the results of lattice simulations using two different lattices [7], given by the light blue and yellow bands. In the lattice simulations,

$m_\pi = 135$  MeV and  $f_\pi = 90$  MeV were used. In this range of isospin chemical potentials,  $\chi$ PT and the quark-meson model are in good qualitative agreement with the lattice data. although the peak in  $c_s^2$  occurs much earlier than in the QM model (See Fig. 6).

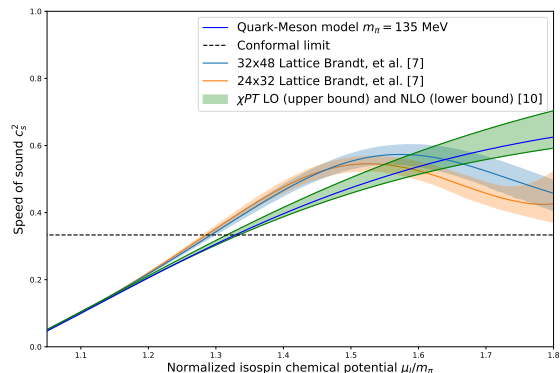


FIG. 5. Speed of sound squared in the pion-condensed phase versus  $\mu_I/m_\pi$ . See main text for details.

In Fig. 6, we show the result for the speed of sound squared  $c_s^2$  using the QM model for a wide range of values for  $\mu_I/m_\pi$  (blue line). The green band is the  $\chi$ PT result [10] obtained as explained above. The red band is the result of the lattice simulations of Ref. [9] with  $m_\pi = 139.6$  MeV and  $f_\pi = 92$  MeV. The band was constructed from 2000 bootstrap samples with  $\pm$  two standard deviation from the mean. The yellow band is the result of the calculations in Ref. [45]. The authors calculated the speed of sound and trace anomaly using the Cornwall-Jackiw-Tomboulis formalism [46], including the gap in their two-loop calculations. Their band is obtained by varying the renormalization scale  $\Lambda = X\mu$  with  $X = 1$  to  $X = 3$ . Our results show that  $c_s^2$  increases sharply from the onset of pion condensation at  $\mu_I = m_\pi$  with a peak at  $\mu_I \approx 335$  MeV. After the peak, the speed of sound relaxes to the conformal limit (shown as the black dashed line). As pointed out in Ref. [41], the overall good agreement with lattice data over a wide range of isospin densities is remarkable. It is also in qualitative agreement with the perturbative calculation of [45].

In Fig. 7, we show the speed of sound squared  $c_s^2$  as a function of the quark chemical potential. The red lines correspond to data set 1 and the blue lines refer to data set 2. Dashed lines are without electric and color charge neutrality, and solid lines are with. Imposing neutrality reduces the speed of sound for all values of  $\mu$ . Moreover, the peak of  $c_s^2$  moves to larger values of  $\mu$  and the peak is also lower. Thus, requiring charge neutrality softens the equation of state. The peak of  $c_s^2$  has also been found in quarkyonic matter [48]. We emphasize that this property and the relaxation to the conformal limit from above are generic features of the QMD model. Regarding the latter, the perturbative treatment of Ref. [45], on

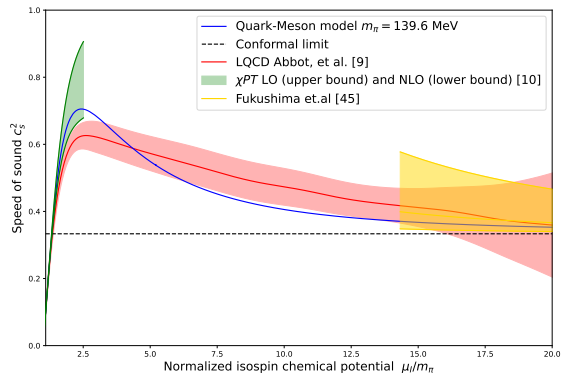


FIG. 6. Speed of sound squared in the pion-condensed phase versus  $\mu_I/m_\pi$ . The pion mass is  $m_\pi = 139.6$  MeV from [9]. See main text for details.

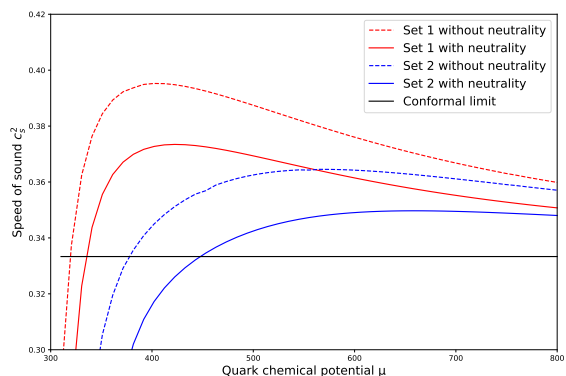


FIG. 7. Speed of sound squared in the 2SC phase for parameter set 1 (red) and set 2 (blue) versus  $\mu$ . Dashed lines are without charge neutrality and solid lines are with charge neutrality. See main text for details.

the other hand, predicts that the conformal limit is approached from below. The peak of the speed of sound is particularly interesting in view of recent neutron star observations. Using agnostic approaches, Refs. [49, 50] find a peak, whereas Ref. [51] observes a plateau as baryon density increases. It is possible to confront QMD model calculations with observation. Combining mass-radius measurements of neutron stars combined with Bayesian inference [52, 53], it is possible to find the probability

distributions of its parameters.

Since we are interested in applying the QMD model to compact stars, we briefly discuss different possibilities for hybrid stars, i.e. stars with a core of deconfined quarks. In a compact star, a possible scenario is several phase transitions as we increase the baryon density. The first transition is from hadronic matter to normal quark matter. The second transition is from normal quark matter to a color superconducting phase. Whether this transition is to the 2SC phase or directly to the CFL depends on the details of the models (masses and couplings) and is an open question. One can ask the question whether the transition is sharp or is it via a mixed phase. A sharp transition takes place at a specific value for the quark chemical potential at which the pressures of the two phases are equal. In each phase, neutrality constraints are imposed locally. The existence of a mixed phase requires a first-order transition between the two phases. In such a two-component system, neutrality constraints are imposed globally [54]. This means that the system is overall neutral with respect to the relevant conserved charges, but one component is positively charged and the other is negatively charged. Following Ref. [55], we consider the possibility of a mixed phase of normal quark matter and 2SC matter. Since normal quark matter is neutral with respect to the color charge  $Q_8$ , we also impose  $\frac{\partial \Omega_{0+1}}{\partial \mu_8} = 0$  on the 2SC phase. If the density in the core of the star is not too high, it is possible that it contains a mixture of normal quark matter and 2SC matter, that is, a non-strange hybrid star is realized. If the density in the core is sufficiently high, one expects a transition to the CFL phase, so we need to extend the QMD model to three flavors. Work in these directions is in progress [56].

## ACKNOWLEDGEMENTS

The authors thank B. Brandt et al. [7], R. Abbott et al. [9], and K. Fukushima [45] for permission to use their lattice data. J. O. A. would also thank B. Brandt, G. Endrodi, and L. von Smekal for useful discussions.

*Note added:* In the final stages of this work, Ref. [41] appeared. Their analysis of the pion-condensed phase and comparison with lattice simulations are similar to those of ours.

[1] K. Rajagopal and F. Wilczek, At the frontier of particle physics, Vol. 3 (World Scientific, Singapore, p 2061) (2001).  
 [2] M. G. Alford, A. Schmitt, K. Rajagopal, and T. Schäfer, Rev. Mod. Phys. **80**, 1455 (2008).

[3] K. Fukushima and T. Hatsuda, Rept. Prog. Phys. **74**, 014001 (2011).  
 [4] D. T. Son and M. A. Stephanov, Phys. Rev. Lett. **86**, 592 (2001).  
 [5] J. Gasser and H. Leutwyler, Ann. Phys. **158**, (142) (1984).

- [6] J. Gasser and H. Leutwyler, Nucl. Phys. B **250**, 465 (1985)
- [7] B. B. Brandt, F. Cuteri, and G. Endrodi, JHEP **07**, 055 (2023).
- [8] R. Abbott et al., NPLQCD Collaboration, Phys. Rev. D **108**, 11, 114506 (2023).
- [9] R. Abbott et al., Phys. Rev. Lett. **134**, 011903 (2025).
- [10] J. O. Andersen, M. K. Johnsrud, Q. Yu, and H. Zhou, Phys. Rev. D **111**, 034017 (2025).
- [11] P. F. Bedaque and T. Schäfer, Nucl. Phys. A **697**, 802 (2002).
- [12] M. Alford and K. Rajagopal, JHEP **06**, 03 (2002).
- [13] S. B. Rüster, V. Werth, M. Buballa, I. A. Shovkovy, and D. H. Rischke, Phys. Rev. D **72**, 034004 (2005).
- [14] H. Abuki and T. Kunihiro, Nucl. Phys. A **768**, 118 (2006).
- [15] T. Gorda, A. Kurkela, P. Romatschke, S. Säppi, and A. Vuorinen, Phys. Rev. Lett. **121**, 202701 (2018).
- [16] T. Gorda, R. Paatelainen, S. Säppi, and K. Seppänen, Phys. Rev. Lett. **131**, 181902 (2023).
- [17] L. Fernandez and J.-L. Kneur, Phys. Rev. Lett. **129**, 212001 (2022); e-Print: 2408.16674 [hep-ph].
- [18] J. O. Andersen and M. P. Nødtvedt, e-Print: 2408.12361 [hep-ph].
- [19] I. A. Shovkovy, Found. Phys. **35**, 1309 (2005).
- [20] A. Gerhold and A. Rebhan, Phys. Rev. D **68**, 011502 (2003).
- [21] D. D. Dietrich, and D. H. Rischke, Prog. Part. Nucl. Phys. **53**, 305 (2004).
- [22] I. A. Shovkovy and M. Huang, Phys. Lett. B **564**, 205 (2003).
- [23] R. Casalbuoni, Z. Duan, and F. Sannino, Phys. Rev. D **62**, 094004 (2000).
- [24] D. Blaschke, D. Ebert, K. G. Klimenko, M. K. Volkov, and V. L. Yudichev, Phys. Rev. D **70**, 014006 (2004).
- [25] H. B. Nielsen and S. Chadha, Nucl. Phys. B **105**, 445 (1976).
- [26] H. Watanabe and H. Murayama, Phys. Rev. Lett. **108**, 251602 (2012).
- [27] Y. Hidaka, Phys. Rev. Lett. **110**, 091601 (2013).
- [28] A. Ncolis, R. Penco, F. Piazza, and R. A. Rosen, JHEP **11**, 055 (2013).
- [29] H. Watanabe, T. Brauner, and H. Murayama, Phys. Rev. Lett. **111**, 021601 (2013).
- [30] T. Brauner, *Effective Field Theory for Spontaneously Broken Symmetry*, Lect. Notes Phys. 1023 (2024).
- [31] T. Schäfer, D. T. Son, and M. A. Stephanov, D. Toublan, J. J. M. Verbaarschot, Phys. Lett. B **522**, 67 (2001).
- [32] A. Ncolis and F. Piazza, Phys. Rev. Lett. **110**, 011602 (2013), *ibid* **110**, 039901 (2013) (addendum).
- [33] P. F. Bedaque, Nucl. Phys. A **697**, 569 (2002).
- [34] L.-Y. He, M. Jin, and P.-F. Zhuang, Phys. Rev. D **71**, 116001 (2005).
- [35] K. Kamikado, N. Strodthoff, L. von Smekal, and J. Wambach, Phys. Lett. B **718** (1044) (2013).
- [36] J. O. Andersen and P. Kneschke, Phys. Rev. D **97**, 076005 (2018).
- [37] A. Ayala, A. Bandyopadhyay, R. L. S. Farias, L. A. Hernández, and J. L. Hernández, Phys. Rev. D **107**, 074027 (2023).
- [38] R. Chiba and T. Kojo, Phys. Rev. D **109**, 076006 (2024).
- [39] A. Ayala, B. S. Lopes, R. L. S. Farias, and L. C. Parra, e-Print: 2409.19406 [hep-ph].
- [40] J. P. Carlomagno, D. G. Dumm, and N. N. Scoccola, Phys. Rev. D **109**, 9, 094041 (2024).
- [41] B. B. Brandt, V. Chelnokov, G. Endrodi, G. Marko, D. Scheid, and L. von Smekal, e-Print: 2502.04025 [hep-ph].
- [42] A. W. Steiner, S. Reddy, and M. Prakash, Phys. Rev. D **66**, 094007 (2002).
- [43] A. Kurkela, K. Rajagopal, and R. Steinhorst, Phys. Rev. Lett. **132**, 26, 262701 (2024).
- [44] M. Huang, P.-F. Zhuang, and W.-Q. Chao, Phys. Rev. D **67**, 065015 (2003).
- [45] K. Fukushima and S. Minato, e-Print: 2411.03781 [hep-ph].
- [46] J. M. Cornwall, R. Jackiw, and E. Tomboulis, Phys. Rev. D **10**, 2428 (1974).
- [47] G. Baym, T. Hatsuda, T. Kojo, P. D. Powell, Y. Song, and T. Takatsuka, Rept. Prog. Phys. **81**, 056902 (2018).
- [48] L. McLerran and S. Reddy, Phys. Rev. Lett. **122**, 122701 (2019).
- [49] S. Altiparmak, C. Ecker, and L. Rezzolla, Astrophys. J. Lett. **939**, L34 (2022).
- [50] M. Marczenko, L. McLerran, K. Redlich, and C. Sasaki, Phys. Rev. C **107**, 025802 (2023).
- [51] L. Brandes, W. Weise, and N. Kaiser, Phys. Rev. D **108**, 094014 (2023).
- [52] M. Albino, T. Malik, M. Ferreira, and C. Providência, Phys. Rev. D **110**, 083037, (2024).
- [53] A. Ayriyan, D. Blaschke, J. P. Carlomagno, G. A. Contrera, and A. G. Grunfeld, e-Print:2501.00115 [nucl-th].
- [54] N. K. Glendenning, Phys. Rev. D **46**, 1274 (1992).
- [55] I. A. Shovkovy, M. Hanauske, and M. Huang, Phys. Rev. D **67**, 103004 (2003).
- [56] J. O. Andersen and N. P. Nødtvedt, Work in progress.